International Journal of Nanomedicine

Dovepress
open access to scientific and medical research

Open Access Full Text Article

ORIGINAL RESEARCH

Recombinant high-density lipoprotein nanoparticles containing gadolinium-labeled cholesterol for morphologic and functional magnetic resonance imaging of the liver

This article was published in the following Dove Press journal:
International Journal of Nanomedicine
16 July 2012
Number of times this article has been viewed

Mengjie Rui[1]
Wei Guo[2]
Qian Ding[2]
Xiaohui Wei[2]
Jianrong Xu[3]
Yuhong Xu[2]

[1]School of Life Science and Biotechnology, [2]School of Pharmacy, Shanghai Jiao Tong University, Shanghai, People's Republic of China; [3]Department of Radiology, Renji Hospital Affiliation with Medical School of Shanghai Jiao Tong University, Shanghai, People's Republic of China

Background: Natural high-density lipoproteins (HDL) possess important physiological functions to the transport of cholesterol from the peripheral tissues to the liver for metabolic degradation and excretion in the bile.

Methods and results: In this work, we took advantage of this pathway and prepared two different gadolinium (Gd)-DTPA-labeled cholesterol-containing recombinant HDL nanoparticles (Gd-chol-HDL) and Gd-$(chol)_2$-HDL as liver-specific magnetic resonance imaging (MRI) contrast agents. The reconstituted HDL nanoparticles had structural similarity to native HDL, and could be taken up by HepG2 cells via interaction with HDL receptors in vitro. In vivo MRI studies in rats after intravenous injections of 10 μmol gadolinium per kg of recombinant HDL nanoparticles indicated that both nanoparticles could provide signal enhancement in the liver and related organs. However, different T_1-weighted image details suggested that they participated in different cholesterol metabolism and excretion pathways in the liver.

Conclusion: Such information could be highly useful to differentiate functional changes as well as anatomic differences in the liver. These cholesterol-derived contrast agents and their recombinant HDL preparations may warrant further development as a new class of contrast agents for MRI of the liver and related organs.

Keywords: magnetic resonance imaging, apolipoprotein, high-density lipoprotein, contrast agent, gadolinium, liver

Introduction

Magnetic resonance imaging (MRI) is a powerful tool used for noninvasive clinical diagnosis. It can provide high-resolution images for delineation of various organ and tissue structures and detection of lesions.[1] In many studies, contrast agents are necessary to highlight differences in histodensity. The most commonly used ones include paramagnetic gadolinium (Gd)-based chelating agents such as Gd(III)-diethylenetriamine penta-acetic acid (Gd-DTPA) and Gd(III)-1,4,7,10-tetracarboxymethyl-1, 4,7,10-tetraazacylododecane (Gd-DOTA).[2] However, these agents are not very good at differentiating diseased (or malfunctioning) tissues from normal ones, because they circulate and distribute nonspecifically throughout the body after injection and would be eliminated quickly by glomerular filtration.[3–5] Thus, there is a great need for development of more sensitive and target-specific functional contrast agents to improve the accuracy of diagnosis using MRI.

Correspondence: Jianrong Xu
Department of Radiology, Renji Hospital, affiliated to Medical School of Shanghai Jiaotong University, 1630 Dongfang Road, Shanghai, 200127, People's Republic of China
Tel +86 21 5875 2345 Ext3059
Fax +86 21 6373 6075
Email xujianr@hotmail.com

Yuhong Xu
School of Pharmacy, Shanghai Jiaotong University, 800 Dongchuan Road, Shanghai, 200240, People's Republic of China
Tel +86 21 3420 4738
Fax +86 21 3420 4738
Email yhxu@sjtu.edu.cn

Lipoproteins are a family of spherical macromolecular particles with the common structure of a hydrophobic core surrounded by a lipid monolayer embedded with apolipoproteins and cholesterols.[6] They are characterized into several classes based on their composition and mass density. Low-density lipoprotein (LDL) and high-density lipoprotein (HDL) are the most extensively studied lipoproteins. Significant efforts have been devoted to the use of recombinant lipoprotein-like nanoparticles as drug delivery vehicles and diagnostic agents, because most of these particles resemble natural lipoprotein structures and are considered highly biocompatible and safe.[7–12]

While most LDL-like nanoparticles have been studied as drug delivery or imaging agents for malignant cells expressing LDL receptors,[13] HDL nanoparticles have been used to target hepatocytes and atherosclerotic plaque because the natural function of HDL is to transport cholesterol from the peripheral tissues to the liver through the reverse cholesterol transport pathway.[14] Frias et al prepared HDL-like nanoparticles containing gadolinium-DTPA-conjugated phospholipid and apolipoprotein A-I (apoA-I) proteins or apoA-I mimetic peptides, 18A and 37pA.[15,16] These HDL-like nanoparticles were shown to bind to atherosclerotic plaque during in vivo MRI experiments. Other studies have incorporated solid nanoparticles of gold, iron oxide, and quantum dots with apoA-I and lipid shells in order to achieve multifunctional imaging of atherosclerotic plaques.[17,18] Fewer papers have explored the localization of reconstituted HDL in the liver. Sriram et al modified apoA-I protein with Gd [MTS-ADO3A] labeling, and found increases in MRI signals in the liver as well as in the kidney.[19] Enhancement of the liver signal was hypothesized to be partly due to the blood pool contrast effect. In addition, because the mean plasma residence time of apoA-I is estimated to be 4–5 days,[20,21] the complexes circulating throughout the plasma may release free gadolinium ions, which are highly toxic and induce many adverse reactions.[22]

In the present study, we attempted to exploit further the specific binding between reconstituted HDL nanoparticles and HDL receptors in the liver, and the cholesterol metabolism pathway. Two cholesterol-conjugated Gd-DTPA complexes with different chemical structures were synthesized, incorporated into recombinant HDL nanoparticles, and named Gd-chol-HDL and Gd-$(chol)_2$-HDL, respectively. These reconstituted HDL nanoparticles were evaluated in terms of morphology, T_1 relaxivity, hepatocyte binding, and in vivo MRI. Gd-chol-HDL and Gd-$(chol)_2$-HDL were both found to be able to improve liver MRI contrasts, but indicated different metabolic properties of the liver.

Materials and methods

Materials

Cholesterol chloroformate, *N*,*N*-diisopropylethylamine, diethylenetriamine penta-acetic acid (DTPA) dianhydride, gadolinium chloride hexahydrate ($GdCl_3 \cdot 6H_2O$), anhydrous dimethyl sulfoxide, tris(hydroxymethyl)aminomethane (Tris), and sodium cholate were purchased from Sigma-Aldrich (St Louis, MO). Anhydrous dichloromethane, concentrated ammonium hydroxide (NH_4OH, containing 30% ammonia), sodium hydroxide (NaOH), spectroscopy-grade acetonitrile (MeCN), sodium bromide (NaBr), sodium chloride (NaCl), and monobasic and dibasic sodium phosphate were purchased from Sinopharm Chemical Reagent Co, Ltd (Shanghai, China). Arsenazo III was purchased from Tokyo Chemical Industries (Tokyo, Japan). 1,2-Dimyristoyl-sn-glycero-3-phosphocholine (DMPC) was sourced from Avanti Polar Lipids (Alabaster, AL). RPMI 1640 medium (supplemented with glutamine and containing phenol red), antibiotics, fetal bovine serum, and 0.25% trypsin-ethylenediamine tetraacetic acid were obtained from Invitrogen (Carlsbad, CA). Deionized water was obtained from a Milli-Q water purification system (Millipore, Billerica, MA). Recombinant human apoA-I was expressed in *Escherichia coli* and purified using His-Trap nickel affinity chromatography, as described by Ryan et al.[23]

The ^1H and ^{13}C nuclear magnetic resonance (NMR) spectra were obtained using a 400 MHz Avance III spectrometer. The chemical shifts were recorded in δ (ppm) and referenced to the solvent or tetramethylsilane. High-resolution mass spectra were recorded using a Waters Premier quadrupole-time-of-flight (Q-Tof) mass spectrometer in negative mode.

Preparation of gadolinium-labeled recombinant HDL nanoparticles

N′-cholesteryloxy-3-carbonyl-1,2-diaminoethane **3** was synthesized by coupling an amine carrying linker **1** to cholesterol through a reaction with cholesterol chloroformate **2**.[24] DTPA bisanhydride **4** (714 mg, 2 mmol) was dissolved in 50 mL of anhydrous dimethyl sulfoxide. Then *N*,*N*-diisopropylethylamine (348 μL, 2 mmol) was added to the solution. *N*′-cholesteryloxy-3-carbonyl-1,2-diaminoethane **3** (472 mg, 1 mmol) was predissolved in anhydrous dichloromethane. While being stirred, the solution was added dropwise into the DTPA bisanhydride solution for 30 minutes under nitrogen in an ice bath. The mixture was then stirred for one day at room temperature. The organic solvent was removed by rotary evaporation, and the residue was stirred

in water at 80°C for 3 hours to dissolve any excess DTPA bisanhydride. The insoluble residue was filtered and dried under vacuum overnight. The crude solid was redissolved in dichloromethane and loaded onto a silica column (dichloromethane/MeOH/NH_3 3:1:0.2 to 1:1:0.2, v/v/v). The desired fractions were pooled and dried to obtain DTPA-cholesterol **5** (360 mg, 43%) and DTPA-(cholesterol)$_2$ **6** (402 mg, 62%).

DTPA-cholesterol **5** was obtained as a pale yellow solid. ^{1}H NMR (400 MHz, $CDCl_3$ + drops of CD_3OD): δ = 0.64 (s, 3H, H-18′, CH3), 0.82 (d, 3H, H-27′, CH_3), 0.83 (d, 3H, H-26′, CH_3), 0.87 (d, 3H, H-21′, CH_3), 0.96 (s, 3H, H-19′, CH_3), 1.01–1.69 (m, 21H, 1-CH_2, 9-CH, 11-CH_2, 12-CH_2, 14-CH, 15-CH_2, 16-CH_2, 17-CH, 20-CH, 22-CH_2, 23-CH_2, 24-CH_2, 25-CH), 1.71–2.04 (m, 5H, 2-CH_2, 7-CH_2, 8-CH), 2.17–2.30 (m, 2H, H-4′, CH_2), 2.54–2.79 (m, 4H, 2 × N-CH_2), 3.13–3.27 (m, 4H, 2 × N-CH_2), 3.36–3.53 (brs, 14H, 5 × N-CH_2-CO, 2 × NH-CH_2), 4.38 (s, 1H, H-3′), 5.31 (s, 1H, H-6′). ^{13}C NMR (400 MHz, $CDCl_3$ + drops of CD_3OD): δ = 11.78, 18.64, 19.23, 20.99, 22.45, 22.71, 23.81, 24.22, 27.94, 28.16, 29.62, 31.81, 35.75, 36.14, 36.50, 36.92, 38.55, 39.45, 39.68, 42.26, 49.98, 56.14, 56.65, 74.45, 122.50, and 139.69. High-resolution mass spectra calculated for $C_{44}H_{72}N_5O_{11}$[M-H$^+$]$^-$ 846.5228 found 846.5253.

DTPA-(cholesterol)$_2$ **6** was obtained as a white solid. ^{1}H NMR (400 MHz, $CDCl_3$ + drops of CD_3OD): δ = 0.64 (s, 6H, H-18′, CH_3), 0.82 (d, 6H, H-27′, CH_3), 0.83 (d, 6H, H-26′, CH_3), 0.87 (d, 6H, H-21′, CH_3), 0.96 (s, 6H, H-19′, CH_3), 1.01–1.69 (m, 42H, 1-CH_2, 9-CH, 11-CH_2, 12-CH_2, 14-CH, 15-CH_2, 16-CH_2, 17-CH, 20-CH, 22-CH_2, 23-CH_2, 24-CH_2, 25-CH), 1.71–2.04 (m, 10H, 2-CH_2, 7-CH_2, 8-CH), 2.17–2.34 (m, 4H, H-4′, CH_2), 2.56–2.70 (brs, 4H, 2 × N-CH_2), 3.1–3.2 (s, 4H, 2 × N-CH_2), 3.22–3.33 (brs, 18H, 5 × N-CH_2-CO, 4 × NH-CH_2), 4.38 (s, 2H, H-3′), 5.31 (s, 2H, H-6′). ^{13}C NMR (400 MHz, $CDCl_3$ + drops of CD_3OD): δ = 11.78, 14.02, 18.63, 19.23, 20.98, 22.47, 22.63, 22.73, 23.81, 24.22, 27.95, 28.17, 29.64, 31.79, 35.76, 36.13, 36.50, 36.92, 38.52, 39.45, 39.68, 42.25, 49.97, 56.12, 56.64, 74.56, 122.50, and 139.71. High-resolution mass spectra calculated for $C_{74}H_{122}N_7O_{12}$[M-H$^+$]$^-$ 1300.9151 found 1300.9171.

Preparation of gadolinium complexes

DTPA-cholesterol **5** (360 mg, 0.425 mmol) was suspended in 30 mL of distilled H_2O. Next, 2 N of NaOH was added to the suspension to dissolve the DTPA-cholesterol. Gadolinium chloride hexahydrate (158 mg, 0.425 mmol) was added dropwise to the mixture and stirred at 60°C for 3 hours. Then, 18 mL of MeCN was added to the mixture, and the precipitate was filtered and dried. The crude solid was purified using a silica column (dichloromethane/MeOH/NH_3 5:1:0.2, v/v/v) to obtain complex **7** as a white solid (92 mg, 21.6% yield). High-resolution mass spectra calculated for $C_{44}H_{69}N_5O_{11}Gd$ [M-Na$^+$]$^-$ 1001.4235 found 1001.4312.

The gadolinium complexes of DTPA-(cholesterol)$_2$ were synthesized using the same procedure. The crude solid was purified using a silica column (dichloromethane/MeOH/NH_3 3:1:0.2, v/v/v) to obtain complex **8** as a white solid (139 mg, 34.5% yield). High-resolution mass spectra calculated for $C_{74}H_{119}N_7O_{12}Gd$ [M-H$^+$]$^-$ 1455.8158 found 1455.8298.

Preparation of recombinant HDL-containing gadolinium complexes

Gd-DTPA-cholesterol (10 mg) and DMPC (13.5 mg) were dissolved in a 3:1 mixture of chloroform and methanol. Next, the solution was dried into a lipid film under a nitrogen stream. The lipid film was dispersed in 1 mL of Tris-buffered solution (20 mM Tris-HCl, 0.15 M NaCl, pH 8.0), and sodium cholate (8.6 mg), and finally apoA-I protein solution (2.3 mg) was added to the dispersion. The molar ratio of apoA-I to Gd-DTPA-cholesterol to DMPC to sodium cholate was 1:125:250:250. The mixture was incubated at 4°C for 12 hours. The mixture was dialyzed against 2 L of Tris-buffered solution, and changed three times over two days. The final product was named Gd-chol-HDL. The same procedure was also used to synthesize the recombinant HDL containing Gd-DTPA-(cholesterol)$_2$; this product was named Gd-(chol)$_2$-HDL.

The gadolinium-labeled HDL nanoparticles were purified from unreacted lipids or free apoA-I proteins by density gradient ultracentrifugation. About 2 mL of sample were adjusted to a density of 1.386 g/mL by addition of solid NaBr, transferred to a 13 mL centrifuge tube, layered with 3.5 mL (1.386 g/mL) and 6.5 mL (1.006 g/mL) of NaBr solution in sequence, and then centrifuged at 41,000 rpm for 48 hours in a Ti41 rotor. The fraction containing the gadolinium-labeled HDL was collected after centrifugation, dialyzed against 2 L of Tris-buffered solution, and changed three times over 2 days.

Characterization of gadolinium-labeled HDL nanoparticles

Chemical composition analysis

ApoA-I protein concentrations in purified gadolinium-labeled HDL were determined using the fluorescamine method.[25] Briefly, 50 μL of samples were diluted 1:20 with phosphate buffer (0.05 M, pH 7.4). The diluted samples were incubated with 0.5 mL of fluorescamine reagent (0.3 mg/mL in acetonitrile). After 5 minutes of incubation at room temperature in the dark, the fluorescence was measured

at the excitation and emission wavelengths of 390 nm and 475 nm, respectively.

Gadolinium concentrations in the gadolinium-labeled HDL were determined using the arsenazo III method.[26] Briefly, samples were diluted 1:100 with HNO_3 solution (0.1 M HNO_3, 10 mM urea, 0.1% Triton X-100, pH 1.0) to release gadolinium ions. Next, 500 µL of samples were mixed with 500 µL of arsenazo III (100 µg/mL) dissolved in the same buffer. The concentration of gadolinium was then read at 654 nm using a 1 cm cuvette against the gadolinium standard curve between 0 and 25 µM.

Analysis of particle size and zeta potential

The mean particle size, polydispersity index, and zeta potential of Gd-chol-HDL and Gd-$(chol)_2$-HDL were determined by dynamic light scattering using a Zetasizer Nano ZS90 instrument (Malvern Instruments, Malvern, UK). The samples were diluted 1:50 with Tris-buffered solution. All measurements were made three times.

Transmission electron microscopy

After dialyzing against a buffer consisting of 0.125 M ammonium acetate, 2.6 mM ammonium carbonate at pH 7.4, Gd-chol-HDL or Gd-$(chol)_2$-HDL at a protein concentration of 0.1 mg/mL was mixed with a 2% sodium phosphotungstate solution (pH 7.4 in distilled water) at a 1:1 ratio by volume, as described by Forte et al.[27] A droplet was placed on a glow-discharged carbon-coated 200-mesh grid and allowed to sit for one minute. The excess fluid was removed by touching the grid with filter paper. Transmission electron microscopic experiments were carried out on a JEM-2010 instrument linked to a GATAN 794 CCD.

In vitro paramagnetic property measurements and calculations

The longitudinal relaxivities (r_1) were obtained using a Siemens Trio 3T MRI scanner at various gadolinium concentrations (0, 0.02, 0.04, 0.08, 0.15, 0.3, and 0.6 mM) in Tris-buffered solution (20 mM Tris, pH 8.0) at room temperature. The T_1 relaxation times were measured using standard inversion recovery sequences. The inversion time ranged from 23 msec to 9000 msec, with a repetition time of 10,000 msec and an echo time of 7.6 msec. The MRI signal intensities in each region of interest (ROI) were used to fit the following monoexponential formula:

$$M_{TR} = M_o\left(1 - 2e^{-\frac{TR}{T_1}}\right)$$

where M_{TR} represents the measured signal intensity as a function of TI, and M_o represents the signal intensity in the equilibrium state. The longitudinal relaxation time (T_1) values were calculated by fitting inversion recovery curves. Subsequently, the longitudinal relaxivity (r_1) was determined from the slope of $1/T_1$ versus six different gadolinium concentrations.

Cell culture

Human hepatic carcinoma (HepG2) cells were purchased from the Type Culture Collection of Chinese Academy of Sciences, Shanghai. The cells were cultured in RPMI 1640 medium supplemented with 10% (v/v) fetal calf serum, 100 µg/mL penicillin, and 10 µg/mL streptomycin at 37°C in 5% CO_2. The growth medium was changed every 2–3 days. Cells were passaged every 5–7 days when they reached 80%–90% confluence. The cells were trypsinized by 0.25% trypsin + 0.53 mM ethylenediamine tetra-acetic acid solution, and the cell concentration was determined using a hemacytometer. HepG2 cells were seeded into 96-well plates or onto a 100 mm culture dish at a density of 5×10^5 cells/mL for subsequent experiments.

In vitro cell viability test

The HepG2 cells were seeded into 96-well plates and cultured for 24 hours to ensure attachment and 70%–80% confluence. After aspiration of the culture medium, the cells were treated with Gd-chol-HDL or Gd-$(chol)_2$-HDL at gadolinium concentrations ranging from 0.01 mM to 0.5 mM. The cell viability assay was done using a Cell Counting Kit (CCK)-8 according to the manufacturer's instructions (Dojindo Laboratories, Tokyo, Japan). Briefly, 10 µL of CCK-8 were added to each well and incubated for 0.5 hours at 37°C in 5% CO_2. The plates were read on a microplate reader at 450 nm. The absorbance value of control cells incubated with fresh culture medium was defined as 100% viability. The viability of reconstituted HDL was calculated as follows:

$$\text{Cell viability (\%)} = (A_{sample} - A_b)/(A_c - A_b) \times 100$$

where A_{sample} was the absorbance value of cells incubated with reconstituted HDL, A_c was the absorbance value of control cells incubated with fresh culture medium, and A_b was the blank absorbance value of the control cells.

In vitro cellular uptake assay

The HepG2 cells were seeded into 100 mm culture dishes and cultured as previously described. After cells were grown

to 70%–80%, the culture medium was replaced with fresh medium containing Gd-chol-HDL or Gd-$(chol)_2$-HDL at a gadolinium concentration of 20 μM. The cells were incubated for various times and then washed three times with phosphate-buffered solution to remove the unbound Gd-chol-HDL or Gd-$(chol)_2$-HDL. Next, the cells were trypsinized and collected, transferred to 2 mL centrifuge tubes, and centrifuged at 300 × g for 5 minutes to obtain the pellets. Acid digestion of the cell pellets was carried out as previously described.[28] Briefly, 0.3 mL of 70% perchloric acid and 0.6 mL of 28% hydrogen peroxide were added to the pellets, and the tubes were sealed with Teflon tape and incubated at 75°C for 5 hours. After cooling to room temperature, the samples were diluted with 2 mL of deionized water and filtered through a 0.45 μm filter. The gadolinium ion content in the cells was determined using inductively coupled plasma atomic emission spectroscopy (ICP-AES) at 342.247 nm.

The cells were treated with 10 μM of Gd-chol-HDL or Gd-$(chol)_2$-HDL in the presence of natural HDL without the gadolinium complexes for competitive binding experiments. The apoA-I protein concentrations of natural HDL were 1–2 times greater than that of Gd-chol-HDL or Gd-$(chol)_2$-HDL. The concentration of gadolinium in the cells was determined by ICP-AES after incubation for 8 hours as previously described.

In vivo MRI

All of the animal experiment protocols in the present study were approved by the institute's animal care and use committee. In vivo MRI was performed using a Siemens Trio 3T scanner with a 50 mm small mouse coil (Siemens). A fast spin-echo T_1 weight sequence was used for the MRI studies (repetition time 1120 msec, echo time 24 msec, field of view 60 × 60 mm, matrix size 512 × 512, contiguous slice thickness 2 mm).

Normal Sprague-Dawley rats (6–8 weeks old, n = 3) were anesthetized with sodium pentobarbital 40 mg/kg administered intraperitoneally. The rats were injected with gadolinium-labeled HDL (Gd-chol-HDL or Gd-$(chol)_2$-HDL) at 10 μmol of gadolinium per kg through the tail vein. The rat was placed at the center of the small mouse coil geometry with at least 10 mm of surrounding space. The radiofrequency excitation was automatically calibrated before each scan. T_1-weighted images were acquired using the same parameters before and after injection of gadolinium-labeled HDL nanoparticles at 5 minutes and 30 minutes, and at one, 2, and 24 hours. The rats were repositioned between each MRI scan to match the images taken at the various time points. The images were analyzed using ImageJ software (version 1.45F; National Institutes of Health, http://rsbweb.nih.gov/ij/) to measure the signals from various ROI representing the qualitative characterization of the liver parenchyma as well as related organs (Figure 6A and B). Care was taken to avoid inclusion of large vessels with the liver ROI. ROI drawn in the inferior slice corresponded to the content of the adjacent duodenal area. The $ROI_{1–3}$ and $ROI_{4,5}$ were 6 mm and 2 mm in diameter, respectively.

Results

Synthesis of Gd-DTPA-cholesterol and Gd-DTPA-$(cholesterol)_2$

Gd-DTPA-cholesterol **7** and Gd-DTPA-$(cholesterol)_2$ **8** were synthesized in three steps, as shown in Scheme 1. Initially, cholesterol was conjugated with ethylenediamine to generate cholesterylamine **3** using Waterhouse's method.[24] In step 2, DTPA-bisanhydride **4** was reacted with the amine group of cholesterylamine **3** to produce a mixture of DTPA-cholesterol **5** and DTPA-$(cholesterol)_2$ **6**. These two compounds were separately collected by silica gel column chromatography. The chemical identity was confirmed by several analytical techniques, including Q-Tof high-resolution mass spectrometry, and ^1H and ^{13}C NMR (see Figures S1–S4 for NMR spectra). In step 3, each compound was incubated with an equal molar ratio of gadolinium chloride hexahydrate in basic solution to obtain Gd(III)-chelated complexes. The concentrations of free and chelated gadolinium ions in each of the complexes were determined using a modified arsenazo III method. The results indicated no detectable free gadolinium ions, and the purities of Gd-DTPA-cholesterol and Gd-DTPA-$(cholesterol)_2$ were over 99.5%. Compared with water-soluble Gd-DTPA, Gd-DTPA-cholesterol and Gd-DTPA-$(cholesterol)_2$ had very low solubility in water in the neutral pH range because of their lipophilic cholesterol moieties. The low solubility of the complexes limited the formation of self-organized micelles and prevented acquisition of relaxivity in aqueous solution.

Preparation and characterization of gadolinium-labeled HDL

Recombinant HDL nanoparticles containing cholesterol-conjugated Gd-DTPA derivatives were prepared by self-assembly during detergent dialysis. The particles assembled were purified by a NaBr gradient density centrifugation method. These nanoparticles were named Gd-chol-HDL

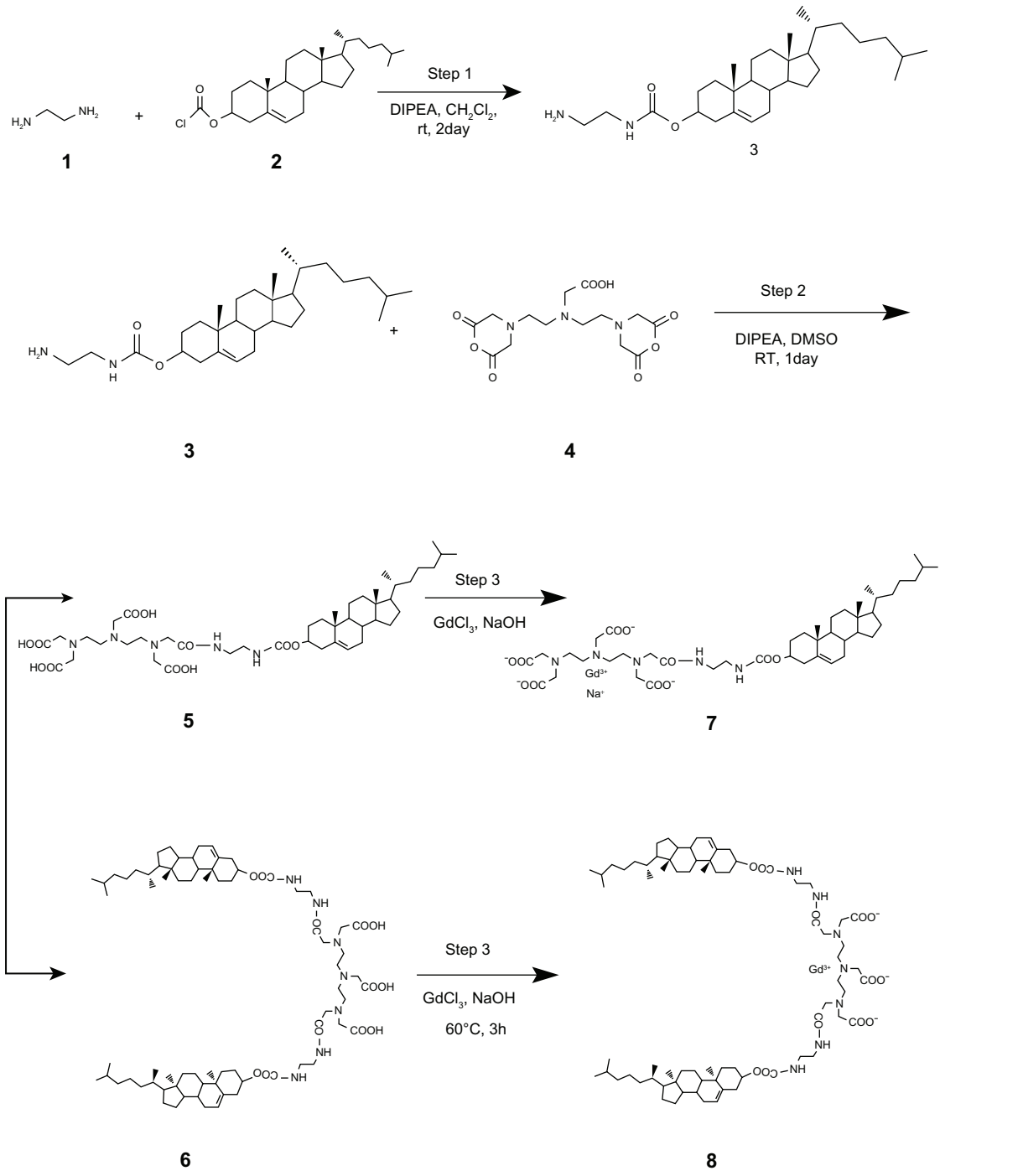

Scheme 1 Route of synthesis for Gd-DTPA-cholesterol and Gd-DTPA-$(cholesterol)_2$.
Abbreviations: Gd, gadolinium; DTPA, diethylenetriamine penta-acetic acid.

and Gd-$(chol)_2$-HDL, respectively. Compositional analysis showed that Gd-chol-HDL had a Gd-DTPA-cholesterol to apoA-I molar ratio of 123.9:1. The ratio for Gd-$(chol)_2$-HDL was 90.7:1, and the incorporation efficiencies of the gadolinium complexes were 99.1% and 72.6%, respectively. The lower gadolinium ratio for Gd-$(chol)_2$-HDL may have been due to the fact that Gd-DTPA-$(cholesterol)_2$ had lower solubility than Gd-DTPA-cholesterol, resulting in significant losses during self-assembly and purification. The resulting molecular assembly structure may be slightly different, as shown in Figure 1.

The size distribution of gadolinium-labeled HDL was determined by dynamic light scattering, and the results are listed in Table 1. The diameter of Gd-$(chol)_2$-HDL was

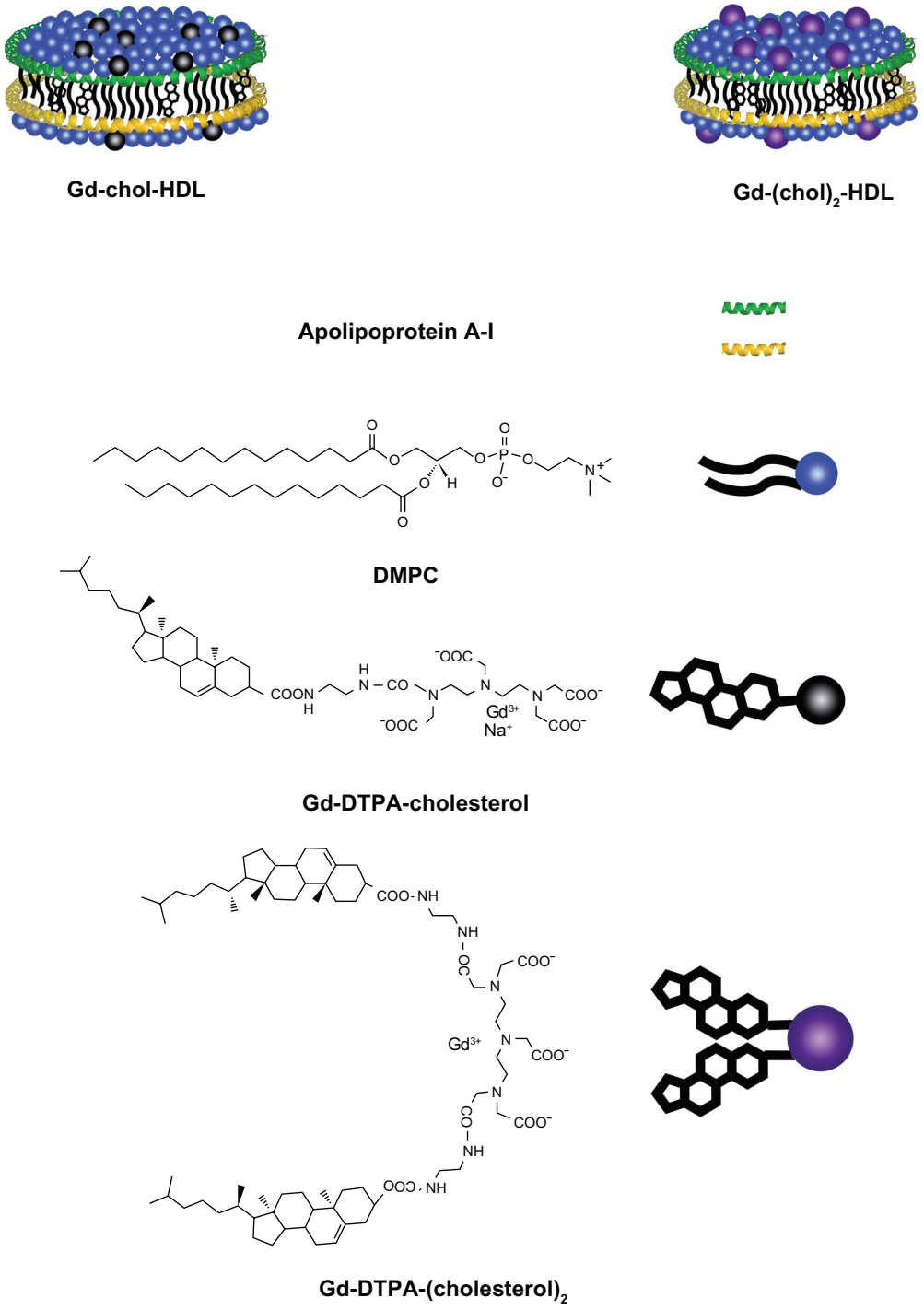

Figure 1 High-density lipoprotein nanoparticles incorporated with cholesterol-based gadolinium complexes.
Abbreviations: Gd, gadolinium; DTPA, diethylenetriamine penta-acetic acid; DMPC, 1,2-dimyristoyl-sn-glycero-3-phosphocholine.

25.54 ± 6.81 nm, and for Gd-chol-HDL was 21.74 ± 5.83 nm. These HDL nanoparticles were well dispersed and had a narrow particle size distribution (Figures S5 and S6). The particle sizes were a little bigger than for natural HDL, which are about 7–13 nm in diameter,[29] but similar to recombinant HDL prepared by the cholate reconstitution method. The size increase may also have been due to the larger hydration radius of the Gd-DTPA moiety on the surface. In a Tris-buffered solution at pH 8.0, Gd-chol-HDL had a lower zeta potential than Gd-$(chol)_2$-HDL (Table 1), presumably because Gd-DTPA-cholesterol was negatively charged and Gd-DTPA-$(cholesterol)_2$ was neutral.

The morphology of Gd-chol-HDL and Gd-$(chol)_2$-HDL was investigated by negative staining transmission

Table 1 Characterization of recombinant HDL nanoparticles

rHDL	Diameter[a] (nm)	PDI[b]	Zeta potential[c] (mV)	Relaxivity[d] r_1 [mM^{-1} s^{-1}]
Gd-chol-HDL	21.74 ± 5.83	0.384	−59.7 ± 26.9	7.67
Gd-$(chol)_2$-HDL	25.54 ± 6.80	0.294	−30.2 ± 5.96	5.16
Gd-DTPA				4.3

Notes: [a]Samples were diluted 1:50 with Tris buffer (pH 8.0) for dynamic light-scattering measurement; [b]PDI is the polydispersity index of rHDL nanoparticles, which corresponds to the square of the normalized standard deviation of an underlying Gaussian size distribution; [c]samples were diluted 1:50 with Tris buffer (20 mM Tris, pH 8.0) for zeta potential measurement; [d]longitudinal relaxivity (r_1) was determined in Tris buffer at 3T on a Siemens clinical magnetic resonance imaging scanner at 25°C. Data of diameter and zeta potential are presented as the mean ± standard deviation, n = 3.
Abbreviations: rHDL, reconstituted high-density lipoprotein; PDI, polydispersity index; Gd, gadolinium; chol, cholesterol; DTPA, diethylenetriamine penta-acetic acid.

electron microscopy. As shown in Figure 2, two distinctively different morphologies for the gadolinium-labeled HDL nanoparticles were evident. Nanoparticles viewed from the top downwards looked like round discs and were thought to be reconstituted HDL, while those viewed from the side looked like rods. These observations were similar to what has already been reported for natural HDL,[27] except that natural HDL would sometimes appear to be stacked into long ribbons when viewed from the side. Very occasionally, there were two discs stacked together. Based on analysis of transmission electron microscopic images of 200 nanoparticles, the calculated average diameters for Gd-chol-HDL and Gd-$(chol)_2$-HDL were 21.98 ± 3.80 nm and 25.11 ± 3.70 nm, respectively. These numbers agreed well with the dynamic light scattering measurements.

Paramagnetic properties of Gd-chol-HDL and Gd-$(chol)_2$-HDL

The relaxivity of Gd-chol-HDL and Gd-$(chol)_2$-HDL nanoparticles in Tris-buffered solution was measured

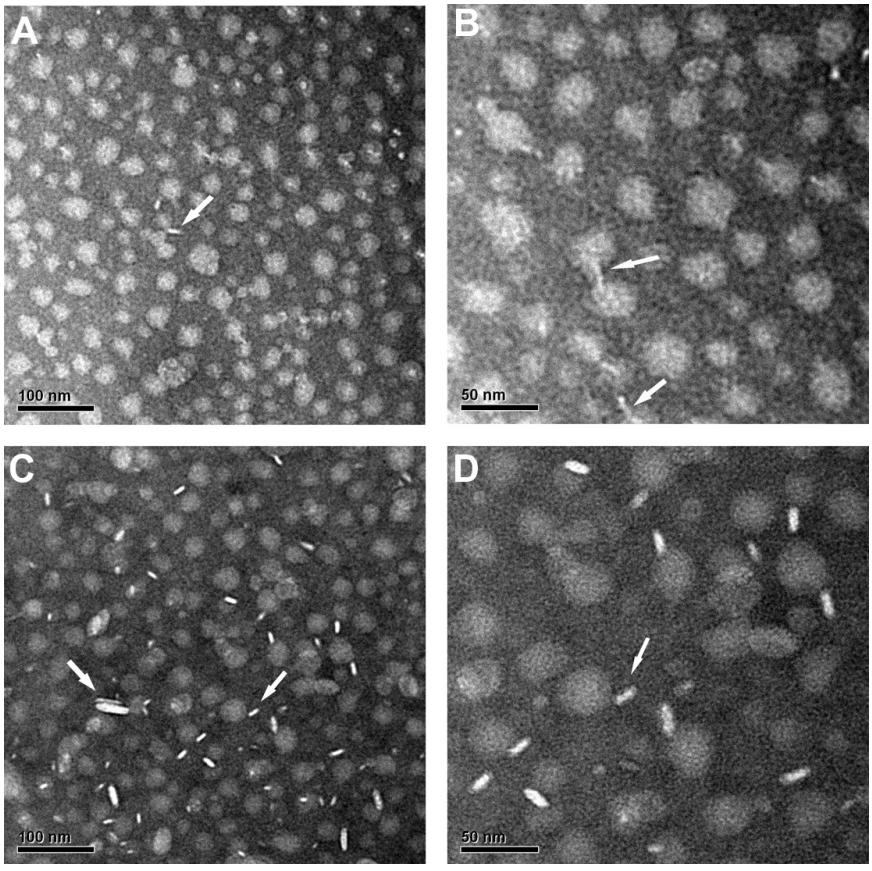

Figure 2 Electron micrographs of negatively stained Gd-chol-HDL (**A** and **B**) and Gd-$(chol)_2$-HDL (**C** and **D**).
Notes: Both samples were stained with 1% sodium phosphotungstate. White arrows indicate that the morphology of Gd-chol-HDL and Gd-$(chol)_2$-HDL are discoidal nanoparticles. Original magnifications: (**A** and **C**) 30,000×, bar = 100 nm; (**B** and **D**) 60,000×, bar = 50 nm.
Abbreviations: Gd, gadolinium; chol, cholesterol; HDL, high-density lipoprotein; DTPA, diethylenetriamine penta-acetic acid.

using a 3T MRI scanner. Typical T_1-weighted spin echo magnetic resonance images of the two nanoparticle solutions at different dilutions are shown in Figure 3A. Gd-DTPA solution was also examined for comparison. The signal intensities from Gd-chol-HDL were the brightest, followed by those from the Gd-$(chol)_2$-HDL samples. Both showed comparatively higher signals than those of Gd-DTPA at the same gadolinium concentrations. Quantitative analysis of the T_1-weighted images confirmed a linear correlation between the longitudinal relaxation rates ($1/T_1$) and gadolinium concentrations. The data were plotted (Figure 3B), and the slopes were fitted to obtain the longitudinal relaxivity (r_1). The r_1 values of Gd-chol-HDL and Gd-$(chol)_2$-HDL were 7.67 mM^{-1} s^{-1} and 5.16 Mm^{-1} s^{-1}, respectively (Table 1). Both r_1 values were significantly higher than that of Gd-DTPA, which was 4.3 mM^{-1} s^{-1}.

In vitro cytotoxicity of reconstituted HDL nanoparticles

The in vitro cytotoxicity of Gd-chol-HDL and Gd-$(chol)_2$-HDL was evaluated using HepG2 cells. The nanoparticles were added into the cell culture medium at different concentrations and incubated for 8 hours. Cell viability were measured after incubation and is reported in Figure 4. Surprisingly, the Gd-chol-HDL nanoparticles produced dose-dependent cytotoxicity, while Gd-$(chol)_2$-HDL and Gd-DTPA remained safe at all concentrations. The 50% growth inhibitory concentration (IC_{50}) of Gd-chol-HDL was 0.356 mM.

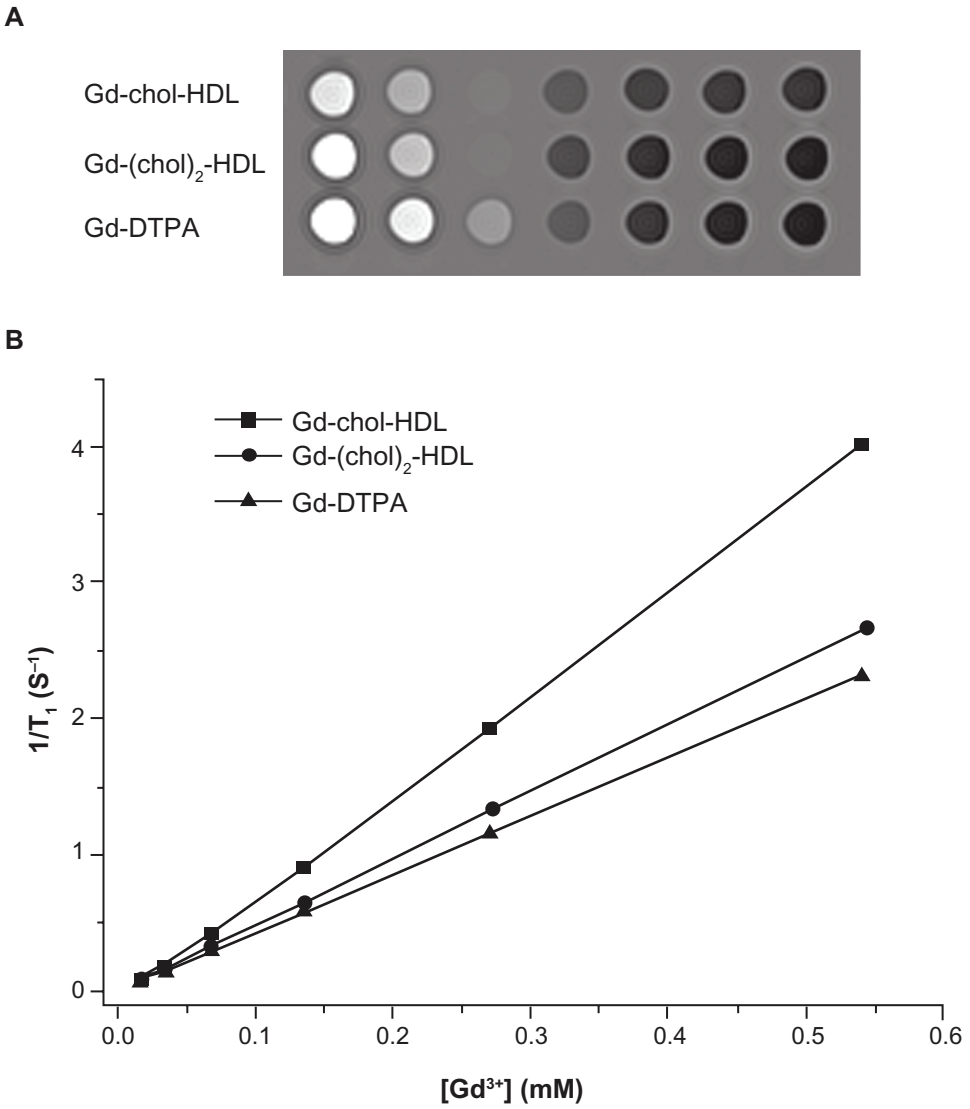

Figure 3 (**A**) In vitro T_1-weighted magnetic resonance images of Gd-chol-HDL, Gd-$(chol)_2$-HDL, and Gd-DTPA in Tris buffers (3T, repetition time/echo time = 10,000/7.6 msec). The gadolinium concentration of each tube was 0.6, 0.3, 0.15, 0.08, 0.04, and 0.02 mM (from left to right), respectively. (**B**) Longitudinal relaxation rates ($1/T_1$) of Gd-chol-HDL, Gd-$(chol)_2$-HDL, and Gd-DTPA in Tris buffer with respect to gadolinium concentration.
Abbreviations: Gd, gadolinium; chol, cholesterol; HDL, high-density lipoprotein; DTPA, diethylenetriamine penta-acetic acid.

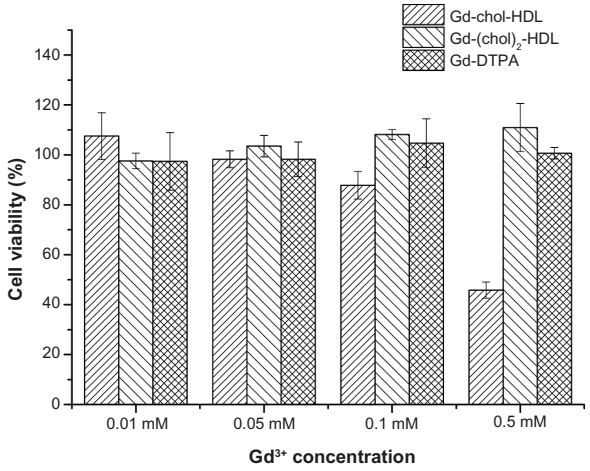

Figure 4 Cell viability of HepG2 cells after incubation with Gd-chol-HDL, Gd-$(chol)_2$-HDL, and Gd-DTPA for 8 hours.
Note: Data represent the mean ± standard deviation (n = 5).
Abbreviations: Gd, gadolinium; chol, cholesterol; HDL, high-density lipoprotein; DTPA, diethylenetriamine penta-acetic acid.

Receptor-mediated uptake of HDL nanoparticles in vitro

Gadolinium-labeled HDL nanoparticles were evaluated for natural HDL receptor-mediated uptake by hepatocytes. As shown in Figure 5A, gadolinium concentration in the cells increased steadily with Gd-chol-HDL incubation. However, the uptake of Gd-$(chol)_2$-HDL was substantially slower in comparison with Gd-chol-HDL. Furthermore, a competitive binding study was carried out in the presence of natural HDL. The protein concentration of the added natural HDL was 1–2 times that of Gd-chol-HDL. We found that the uptake of Gd-chol-HDL was significantly lower when there was more native HDL (Figure 5B).

Morphological and functional imaging of the liver aided by HDL nanoparticles

In vivo MRI of the rat liver and surrounding tissues and organs was performed before and after injection of gadolinium-labeled HDL nanoparticles. Gd-chol-HDL and Gd-$(chol)_2$-HDL were injected into Sprague Dawley rats via the tail vein at a dose of 10 μmol/kg. No visible signs of any adverse reactions were noted after monitoring for 72 hours. MRI images were acquired before and after administration, and for up to 24 hours. After reconstruction of the MRI images, sectional axial-plane images were analyzed and quantified.

The axial sectional images from middle and inferior slices of the liver are shown in Figure 6A and B, respectively. The inferior slice included regions of the descending part of the duodenum, where the bile duct enters the intestine.

As shown in Figure 6A and B, the overall signal intensities of the liver were elevated at various time points after administration of Gd-chol-HDL or Gd-$(chol)_2$-HDL. However, the enhancement trends of the two gadolinium-labeled HDL were different. After injection of Gd-chol-HDL (Figure 6A), the signal from the liver gradually increased for more than 2 hours, and then gradually decreased. At all time points, the overall signal intensities inside the liver remained higher than the preinjection baseline. More interestingly, the signals from the duodenal area demonstrated a steady increase

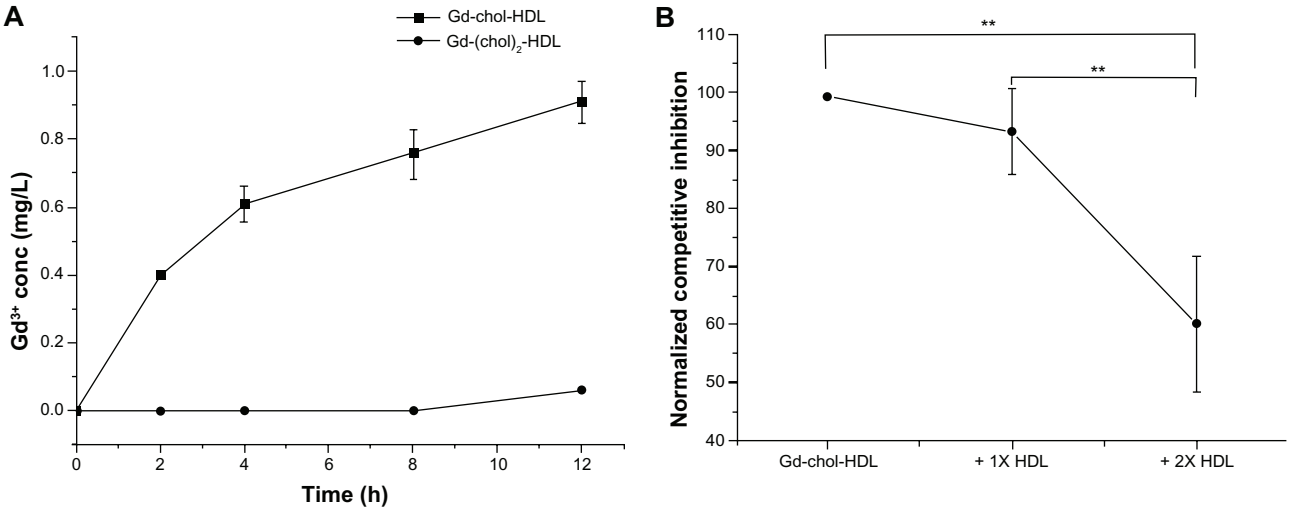

Figure 5 (**A**) Gadolinium uptake curves of Gd-chol-HDL and Gd-$(chol)_2$-HDL in HepG2 cells at a gadolinium ion concentration of 10 μM. (**B**) Competitive inhibition effect of two different apoA-I concentrations of native HDL on uptake of Gd-chol-HDL in HepG2 cells after incubation for 8 hours.
Notes: Bars represent the mean ± standard deviation (n = 3). $^{**}P < 0.005$, significantly different from the value of Gd-chol-HDL.
Abbreviations: Gd, gadolinium; chol, cholesterol; HDL, high-density lipoprotein.

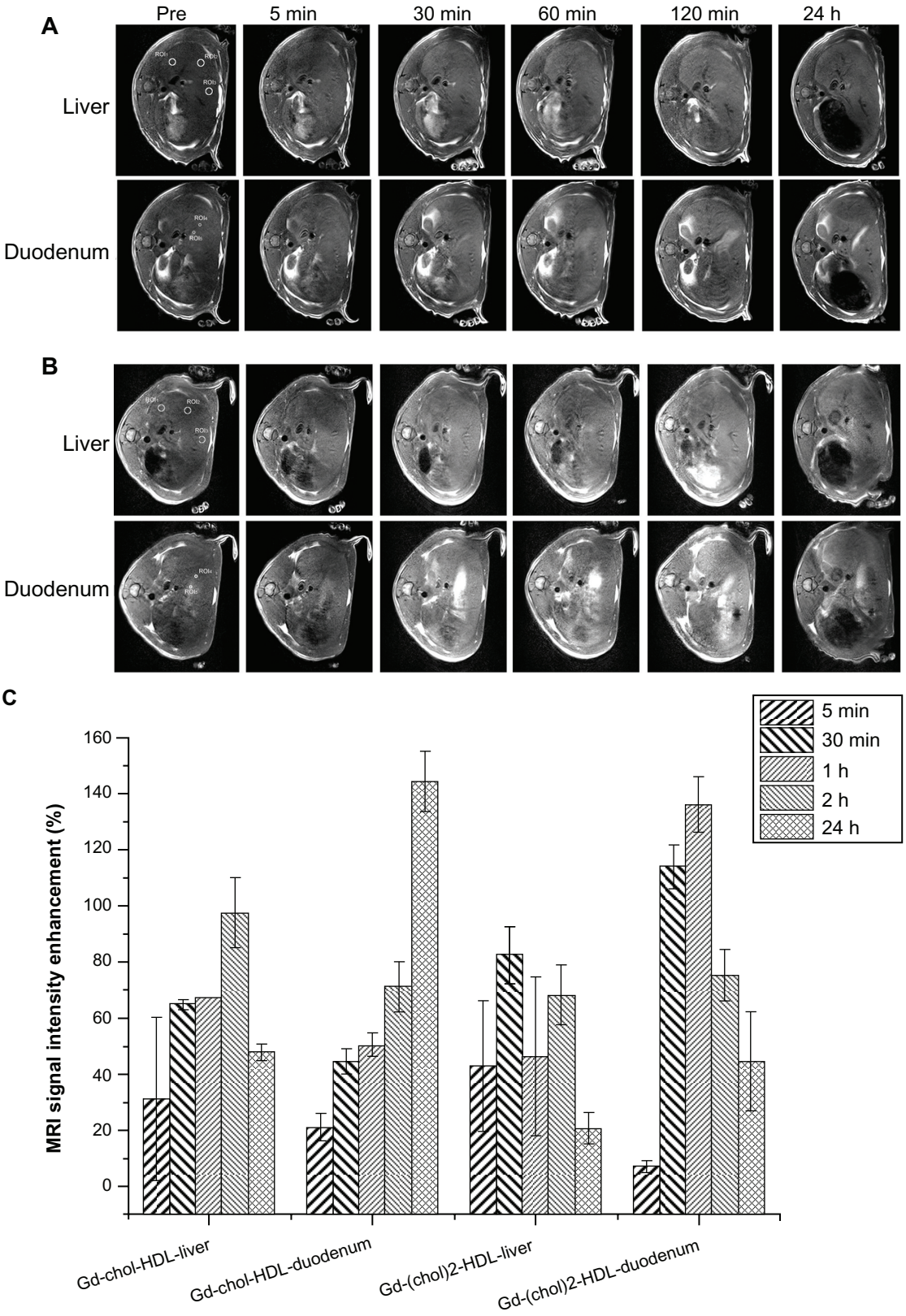

Figure 6 Representative in vivo MRI images of Sprague-Dawley rat liver injected with gadolinium-labeled reconstituted HDL. MRI images were obtained at different time points after injection of 10 μmol/kg (**A**) Gd-chol-HDL or (**B**) Gd-$(chol)_2$-HDL. The five measured ROI used for the time courses in (**A**) and (**B**) are shown in the preinjection images. $ROI_{1–3}$ and $ROI_{4–5}$ were 6 mm and 2 mm in diameter, respectively. (**C**) Intensity enhancement of liver and the surrounding duodenum in vivo after injection of Gd-chol-HDL (n = 3) or Gd-$(chol)_2$-HDL (n = 3).

Note: Bars represent the mean ± standard deviation (n = 3).

Abbreviations: Gd, gadolinium; chol, cholesterol; MRI, magnetic resonance imaging; HDL, high-density lipoprotein; ROI, region of interest.

up to 24 hours. In contrast, after Gd-$(chol)_2$-HDL injection (Figure 6B), some signal enhancement was observed in the liver but this enhancement decreased more rapidly compared with Gd-chol-HDL.

In order for more quantitative analysis of the MRI intensity changes, signals from several ROI were measured using ImageJ software. Five ROI are shown in the preinjection images depicted in Figure 6A and B. The liver ROI were carefully drawn to include only the parenchyma of the right and left lobe of the liver, and the ROI_4 and ROI_5 corresponded to the descending portion of the duodenum. The relative signal enhancement ratio (ER%) was calculated from the following equation:

$$ER\% = (Intensity_{post} - Intensity_{pre}) \times 100\%/Intensity_{pre}$$

and plotted as shown in Figure 6C. After injection of Gd-chol-HDL, magnetic resonance signals increased by almost 100% and lasted for at least 24 hours. Signals from the duodenum increased more gradually and also reached 136.1% signal enhancement at 24 hours after injection. In contrast, after injection of Gd-$(chol)_2$-HDL, liver signals only increased a little overall, but significant signal enhancement from the duodenum and the related hepatobiliary system was observed. The maximum enhancement in liver parenchyma was about 140% at one hour after injection, but overall, significant enhancement lasted for more than 24 hours. Strong signals in the liver and duodenum suggested hepatobiliary activity after administration of Gd-chol-HDL or Gd-$(chol)_2$-HDL.

Discussion

Lipid-based nanoparticles, such as liposomes, micelles, and solid lipid nanoparticles, are being studied extensively as drug carriers or diagnostic agents. Among them, nanoparticles that resemble the structure of natural lipoproteins are considered desirable because they show specific traffic patterns that can be exploited for targeted drug delivery. For example, there have been many successful studies using LDL-like nanoparticles for targeted drug delivery to cancer cells.[7,13,30–35] LDL nanoparticles containing lipophilic gadolinium complexes such as Gd-AAZTAC17 are also utilized as MRI probes for tumor cells in vitro and in vivo.[9] Similarly, many HDL nanoparticles have also been developed as drug or gene delivery systems, with many targeted to the liver, to which natural HDL is targeted.[10,11,36,37]

Hepatocytes express high levels of HDL receptors (scavenger receptor class B, type I, SR-BI) that interact with the apoA-I protein on HDL surfaces. After such interactions, the cholesterol inside HDL is taken up selectively, then excreted into the bile directly or after being metabolized into bile acids. In this study, we took advantage of this cholesterol transportation pathway, and synthesized two cholesterol-based Gd-DTPA derivatives. Both complexes could be incorporated into HDL nanoparticles. The Gd-DTPA-cholesterol complex assembled very efficiently, while the Gd-DTPA-$(cholesterol)_2$ complex was more hydrophobic and could not be completely incorporated after detergent dialysis.

The differences in solubility may cause different molecular assembly structures whereby the Gd-DTPA-$(cholesterol)_2$ molecules sink deeper than Gd-DTPA-cholesterol into the lipophilic core. Therefore, incorporation of nonionic Gd-DTPA-$(cholesterol)_2$ resulted in a less negative zeta potential and slightly larger sizes compared with Gd-DTPA-cholesterol (Table 1). As such, Gd-DTPA-$(cholesterol)_2$ showed a lower water exchange rate between coordinated water and the bulk solvent, and consequently had lower relaxivity. Based on these data and our analysis, we created a schematic representation of the structures of HDL nanoparticles containing Gd-DTPA derivatives, as shown in Figure 1.

HepG2 cells were chosen as the in vitro cell model in our study because they are the best characterized human liver cell line. HepG2 cells are reported to retain many of the physical properties and biological functions of human hepatocytes, including liver metabolism, secretion of plasma proteins, and enzymes.[38–40] In addition, HepG2 cells have been shown to express high levels of HDL receptors that mediate selective uptake of cholesteryl esters (SR-BI) or holoparticle endocytosis (mitochondrial β chain of ATP synthase/P2Y13).[41,42] In the present study, the two Gd-labeled HDL nanoparticles were found to have different uptake properties. The uptake of Gd-chol-HDL was faster and more efficient. However, they were also somewhat cytotoxic, probably because the Gd-DTPA-cholesterol molecules may have detergent-like properties that could disrupt the cell membrane. In fact, the cytotoxicity of Gd-chol-HDL was found to be related to cell incubation time (data not shown). The Gd-$(chol)_2$-HDL nanoparticles were much less toxic because the more hydrophobic Gd-DTPA-$(cholesterol)_2$ molecules were more stably embedded inside the HDL nanoparticles and were less surface-active. However, the uptake kinetics of Gd-$(chol)_2$-HDL were slower, which could also be attributed to the stable incorporation of Gd-DTPA-$(cholesterol)_2$ in HDL.

During in vivo MRI examination, there were no significant adverse reactions observed because the surface-active molecules were easily diluted and the contact time was short. Both Gd-chol-HDL and Gd-$(chol)_2$-HDL resulted in

hepatic tissue contrast enhancement, but their underlying mechanisms could be quite different. A schematic drawing of our proposed HDL uptake and elimination mechanism in vivo is shown in Figure 7. Gd-chol-HDL nanoparticles were taken up quickly by hepatocytes and showed signals in the liver within half an hour after injection. The signal enhancement persisted for a while and then decreased gradually. At the same time, the signal intensity at the duodenum increased slowly. We think that, once inside hepatocytes, Gd-DTPA-cholesterol molecules are slowly metabolized into bile acids, and subsequently excreted into the bile ducts and the small intestine, resulting in signal enhancement in the duodenum for up to 24 hours. In fact, MRI images taken at 2 hours after injection, shown in Figure 6, actually highlight some detailed biliary tract structures inside the liver mass. The gadolinium-labeled bile acids caused specific imaging enhancement in the liver bile duct system. In contrast, Gd-$(chol)_2$-HDL appeared to behave via a different mechanism, as proposed in Figure 7. Some signal enhancements in the liver were observed within 30 minutes after injection. However, because Gd-DTPA-$(cholesterol)_2$ may not be easily taken up and converted into bile acids, it behaved more like a blood pool contrast agent, or could also be directly excreted into the bile via the biliary sterol secretion pathway to add to the duodenum signal. In addition, because the rat is naturally deficient in cholesterol ester transfer protein, we did not evaluate the influence of cholesterol ester transfer protein on the distribution of reconstituted HDL nanoparticles. As a key regulator of cholesterol flux through the reverse cholesterol transport pathway, cholesterol ester transfer protein may promote the transfer of gadolinium complexes from reconstituted HDL to very low-density lipoprotein or LDL, and probably raise the risk of atherosclerosis. However, because of their high relaxivity, the reconstituted HDL nanoparticles can be used at a low dose and may not have a significant impact on LDL-induced oxidative stress. In addition, we think it may not be a suitable substrate for cholesterol ester transfer protein because its structure more closely resembles cholesteryl sulfate, which is actually a cholesterol ester transfer protein inhibitor.[43]

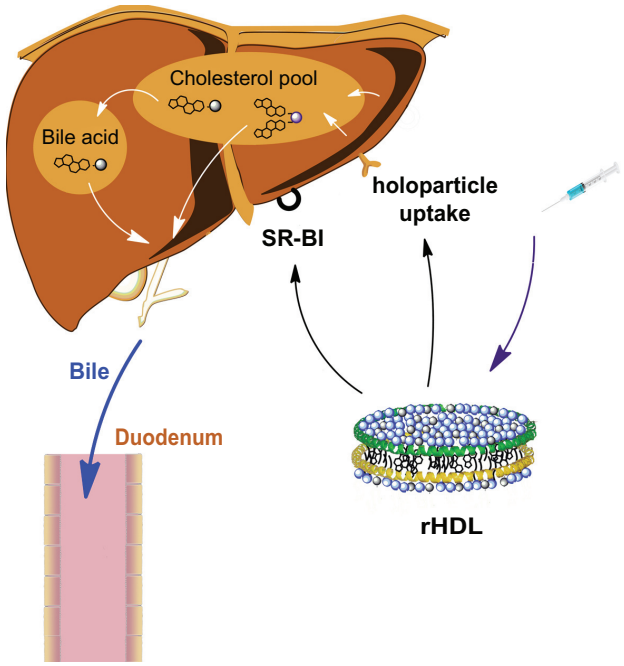

Figure 7 Possible uptake mechanism of Gd-chol-HDL and Gd-$(chol)_2$-HDL nanoparticles. After intravenous injection, discoidal Gd-chol-HDL and Gd-$(chol)_2$-HDL nanoparticles were taken up by the liver through several pathways. The cholesterol-based complexes could be taken up by mediation of SR-BI. In addition, holoparticle uptake by hepatocytes is mediated by the ectopic β-chain of ATP synthase and $P2Y_{13}$ receptors. Gd-DTPA-cholesterol may be converted into bile acids and retained in the liver for a relatively long period of time. The bile acids are then excreted into bile. However, Gd-DTPA-$(cholesterol)_2$ may not be a suitable substrate for enzymes that catalyze the conversion of cholesterol into bile acid. Thus Gd-DTPA-$(cholesterol)_2$ may be excreted into bile directly via the biliary sterol secretion pathway.

Abbreviations: DTPA, diethylenetriamine penta-acetic acid; Gd, gadolinium; chol, cholesterol; MRI, magnetic resonance imaging; HDL, high-density lipoprotein; SR-BI, scavenger receptor class B type I.

The major advantage of these contrast agents over the others reported is that they can participate in specific hepatocyte functions. The most commonly used contrast agents, ie, Gd-DTPA, Gd-DTPA-BMA, and Gd-DOTA, are all extracellular fluid agents that do not enter hepatocytes and accumulate in the liver. Superparamagnetic iron oxide particles are typical T_2 contrast agents, and could be taken up by phagocytic Kupffer cells in the liver and then darken the target tissue in T_2-weighted images.[44] In addition, many reports on developing nanoparticle-based contrast agents also target Kupffer cells, including liposomes, dendrimers, and other polymers.[45–48] There are only a few hepatocyte-specific contrast agents in clinical use, such as Mn-DPDP, Gd-BOPTA, and Gd-EOB-DTPA,[2,49,50] for detecting and characterizing lesions in normal or cirrhotic livers. Among them, Gd-BOPTA and Gd-EOB-DTPA are taken up by hepatocytes through the organic anion transport system, which is normally used for the hepatocellular uptake of bilirubin and has relatively low specificity.[51] Therefore, uptake of Gd-BOPTA and Gd-EOB-DTPA could be inhibited by an increase in serum bilirubin levels and by inhibitors such as bromosulfophthalein and rifampicin.[52,53] In contrast, the gadolinium-labeled HDL nanoparticles we developed were taken up via HDL-receptor mediated pathways, which were not easily blocked and might more efficiently increase the contrast of the liver parenchyma. More importantly, we showed that gadolinium complexes could participate in the hepatic cholesterol metabolic pathway and be excreted into

the bile, which could be of great benefit for assessing the anatomic structure and functions of the biliary tree.

A disease called nephrogenic systemic fibrosis was recently found to be associated with the use of MRI contrast agents such as Gd-DTPA-BMA and Gd-DTPA,[54] because they are eliminated by renal excretion and may trigger nephrogenic systemic fibrosis in patients with kidney disease.[55] The present work showed that Gd-DTPA-cholesterol and Gd-DTPA-$(cholesterol)_2$ could be metabolized into the bile and subsequently secreted via the feces. These Gd-labeled HDL nanoparticles could thus be developed as safer contrast agents, with more detailed studies concerning the exact elimination pathway of these cholesterol-based compounds.

Conclusion

In the present study, the synthesis and characterization of cholesterol-modified Gd-DTPA derivatives and their reconstitution into recombinant HDL nanoparticles were investigated. Both in vitro and in vivo studies showed that the gadolinium-labeled HDL were readily taken up by hepatocytes and efficiently improved the signal intensity of liver tissues and the duodenal area. Our data indicate that gadolinium-labeled HDL nanoparticles might be important and efficient contrast agents for specific imaging of the liver and related organs.

Acknowledgments

We would like to thank Weiwei Men and Dazhi Yin for MRI manipulation at the Shanghai Key Laboratory of Magnetic Resonance, East China Normal University. This research was financially supported by the National Science Foundation of China (30825045).

Disclosure

The authors report no conflicts of interest in this work.

References

1. Caravan P, Ellison JJ, McMurry TJ, Lauffer RB. Gadolinium (III) chelates as MRI contrast agents: structure, dynamics, and applications. *Chem Rev*. 1999;99(9):2293–2352.
2. Geraldes CF, Laurent S. Classification and basic properties of contrast agents for magnetic resonance imaging. *Contrast Media Mol Imaging*. 2009;4(1):1–23.
3. Seale MK, Catalano OA, Saini S, Hahn PF, Sahani DV. Hepatobiliary-specific MR contrast agents: role in imaging the liver and biliary tree. *Radiographics*. 2009;29(6):1725–1748.
4. Langereis S, Dirksen A, Hackeng TM, van Genderen MHP, Meijer EW. Dendrimers and magnetic resonance imaging. *New J Chem*. 2007;31(7):1152–1160.
5. Luo K, Liu G, He B, et al. Multifunctional gadolinium-based dendritic macromolecules as liver targeting imaging probes. *Biomaterials*. 2011;32(10):2575–2585.
6. Rensen PCN, de Vrueh RLA, Kuiper J, Bijsterbosch MK, Biessen EAL, van Berkel TJC. Recombinant lipoproteins: lipoprotein-like lipid particles for drug targeting. *Adv Drug Deliv Rev*. 2001;47(2–3):251–276.
7. Zhou P, Hatziieremia S, Elliott MA, et al. Uptake of synthetic low density lipoprotein by leukemic stem cells – a potential stem cell targeted drug delivery strategy. *J Control Release*. 2010;148(3):380–387.
8. Maximov VD, Reukov VV, Barry JN, Cochrane C, Vertegel AA. Protein-nanoparticle conjugates as potential therapeutic agents for the treatment of hyperlipidemia. *Nanotechnology*. 2010;21(26):265103.
9. Crich SG, Lanzardo S, Alberti D, et al. Magnetic resonance imaging detection of tumor cells by targeting low-density lipoprotein receptors with Gd-loaded low-density lipoprotein particles. *Neoplasia*. 2007;9(12):1046–1056.
10. Zhang X, Chen B. Recombinant high density lipoprotein reconstituted with apolipoprotein AI cysteine mutants as delivery vehicles for 10-hydroxycamptothecin. *Cancer Lett*. 2010;298(1):26–33.
11. Feng M, Cai Q, Huang H, Zhou P. Liver targeting and anti-HBV activity of reconstituted HDL-acyclovir palmitate complex. *Eur J Pharm Biopharm*. 2008;68(3):688–693.
12. Oda MN, Hargreaves PL, Beckstead JA, Redmond KA, van Antwerpen R, Ryan RO. Reconstituted high density lipoprotein enriched with the polyene antibiotic amphotericin B. *J Lipid Res*. 2006;47(2):260–267.
13. Firestone RA. Low-density lipoprotein as a vehicle for targeting antitumor compounds to cancer cells. *Bioconjug Chem*. 1994;5(2):105–113.
14. van der Velde AE. Reverse cholesterol transport: from classical view to new insights. *World J Gastroenterol*. 2010;16(47):5908–5915.
15. Frias JC, Williams KJ, Fisher EA, Fayad ZA. Recombinant HDL-like nanoparticles: a specific contrast agent for MRI of atherosclerotic plaques. *J Am Chem Soc*. 2004;126(50):16316–16317.
16. Cormode DP, Chandrasekar R, Delshad A, et al. Comparison of synthetic high density lipoprotein (HDL) contrast agents for MR imaging of atherosclerosis. *Bioconjug Chem*. 2009;20(5):937–943.
17. Cormode DP, Skajaa T, van Schooneveld MM, et al. Nanocrystal core high-density lipoproteins: a multimodality contrast agent platform. *Nano Lett*. 2008;8(11):3715–3723.
18. Skajaa T, Cormode DP, Jarzyna PA, et al. The biological properties of iron oxide core high-density lipoprotein in experimental atherosclerosis. *Biomaterials*. 2011;32(1):206–213.
19. Sriram R, Lagerstedt JO, Petrlova J, et al. Imaging apolipoprotein AI in vivo. *NMR Biomed*. 2011;24(7):916–924.
20. Roma P, Gregg RE, Meng MS, et al. In vivo metabolism of a mutant form of apolipoprotein A-I, apo A-I Milano, associated with familial hypoalphalipoproteinemia. *J Clin Invest*. 1993;91(4):1445–1452.
21. Malmendier CL, Delcroix C, Ameryckx JP. In vivo metabolism of human apoprotein A-I-phospholipid complexes. Comparison with human high density lipoprotein-apoprotein A-I metabolism. *Clin Chim Acta*. 1983;131(3):201–210.
22. Idee JM, Port M, Raynal I, Schaefer M, Le Greneur S, Corot C. Clinical and biological consequences of transmetallation induced by contrast agents for magnetic resonance imaging: a review. *Fundam Clin Pharmacol*. 2006;20(6):563–576.
23. Ryan RO, Forte TM, Oda MN. Optimized bacterial expression of human apolipoprotein A-I. *Protein Expr Purif*. 2003;27(1):98–103.
24. Waterhouse JE, Harbottle RP, Keller M, et al. Synthesis and application of integrin targeting lipopeptides in targeted gene delivery. *Chembiochem*. 2005;6(7):1212–1223.
25. Funk GM, Hunt CE, Epps DE, Brown PK. Use of a rapid and highly sensitive fluorescamine-based procedure for the assay of plasma lipoproteins. *J Lipid Res*. 1986;27(7):792–795.
26. Nagaraja TN, Croxen RL, Panda S, et al. Application of arsenazo III in the preparation and characterization of an albumin-linked, gadolinium-based macromolecular magnetic resonance contrast agent. *J Neurosci Methods*. 2006;157(2):238–245.
27. Forte TM, Nordhausen RW. Electron microscopy of negatively stained lipoproteins. *Methods Enzymol*. 1986;128:442–457.

28. Tamat SR, Moore DE, Allen BJ. Determination of boron in biological tissues by inductively coupled plasma atomic emission spectrometry. *Anal Chem*. 1987;59(17):2161–2164.
29. Nichols AV, Krauss RM, Musliner TA. Nondenaturing polyacrylamide gradient gel electrophoresis. *Methods Enzymol*. 1986;128:417–431.
30. Maximov VD, Reukov VV, Barry JN, Cochrane C, Vertegel AA. Protein-nanoparticle conjugates as potential therapeutic agents for the treatment of hyperlipidemia. *Nanotechnology*. 2010;21(26):265103.
31. Forte TM, Nikanjam M, Blakely EA, Bjornstad KA, Shu X, Budinger TF. Synthetic nano-low density lipoprotein as targeted drug delivery vehicle for glioblastoma multiforme. *Int J Pharm*. 2007;328(1):86–94.
32. Ji B, Peacock G, Lu DR. Synthesis of cholesterol-carborane conjugate for targeted drug delivery. *Bioorg Med Chem Lett*. 2002;12(17):2455–2458.
33. Chu ACY, Tsang SY, Lo EHK, Fung KP. Low density lipoprotein as a targeted carrier for doxorubicin in nude mice bearing human hepatoma HepG2 cells. *Life Sci*. 2001;70(5):591–601.
34. Callahan DE, Forte TM, Afzal SM, et al. Boronated protoporphyrin (BOPP): localization in lysosomes of the human glioma cell line SF-767 with uptake modulated by lipoprotein levels. *Int J Radiat Oncol Biol Phys*. 1999;45(3):761–771.
35. Vitols S, Soderberg-Reid K, Masquelier M, Sjostrom B, Peterson C. Low density lipoprotein for delivery of a water-insoluble alkylating agent to malignant cells. In vitro and in vivo studies of a drug-lipoprotein complex. *Br J Cancer*. 1990;62(5):724–729.
36. Lee H, Kim SI, Shin D, et al. Hepatic siRNA delivery using recombinant human apolipoprotein A-I in mice. *Biochem Biophys Res Commun*. 2009;378(2):192–196.
37. Feng MQ, Cai QS, Shi XL, Huang H, Zhou P, Guo X. Recombinant high-density lipoprotein complex as a targeting system of nosiheptide to liver cells. *J Drug Target*. 2008;16(6):502–508.
38. Knowles BB, Howe CC, Aden DP. Human hepatocellular carcinoma cell lines secrete the major plasma proteins and hepatitis B surface antigen. *Science*. 1980;209(4455):497–499.
39. Aden DP, Fogel A, Plotkin S, Damjanov I, Knowles BB. Controlled synthesis of HBsAg in a differentiated human liver carcinoma-derived cell line. *Nature*. 1979;282(5739):615–616.
40. Mersch-Sundermann V, Knasmuller S, Wu XJ, Darroudi F, Kassie F. Use of a human-derived liver cell line for the detection of cytoprotective, antigenotoxic and cogenotoxic agents. *Toxicology*. 2004;198(1–3):329–340.
41. Rhainds D, Bourgeois P, Bourret G, Huard K, Falstrault L, Brissette L. Localization and regulation of SR-BI in membrane rafts of HepG2 cells. *J Cell Sci*. 2004;117(Pt 15):3095–3105.
42. Vantourout P, Radojkovic C, Lichtenstein L, Pons V, Champagne E, Martinez LO. Ecto-F-ATPase: a moonlighting protein complex and an unexpected apoA-I receptor. *World J Gastroenterol*. 2010;16(47):5925–5935.
43. Connolly DT, Krul ES, Heuvelman D, Glenn KC. Inhibition of cholesteryl ester transfer protein by apolipoproteins, lipopolysaccharides, and cholesteryl sulfate. *Biochim Biophys Acta*. 1996;1304(2):145–160.
44. Stark DD, Weissleder R, Elizondo G, et al. Superparamagnetic iron oxide: clinical application as a contrast agent for MR imaging of the liver. *Radiology*. 1988;168(2):297–301.
45. Cittadino E, Ferraretto M, Torres E, et al. MRI evaluation of the antitumor activity of paramagnetic liposomes loaded with prednisolone phosphate. *Eur J Pharm Sci*. 2012;45(4):436–441.
46. Luo K, Liu G, She WC, et al. Gadolinium-labeled peptide dendrimers with controlled structures as potential magnetic resonance imaging contrast agents. *Biomaterials*. 2011;32(31):7951–7960.
47. Kobayashi H, Brechbiel MW. Nano-sized MRI contrast agents with dendrimer cores. *Adv Drug Deliv Rev*. 2005;57(15):2271–2286.
48. Chen ZJ, Yu DX, Liu CX, et al. Gadolinium-conjugated PLA-PEG nanoparticles as liver targeted molecular MRI contrast agent. *J Drug Target*. 2011;19(8):657–665.
49. Lee NK, Kim S, Lee JW, et al. Biliary MR imaging with Gd-EOB-DTPA and its clinical applications. *Radiographics*. 2009;29(6):1707–1724.
50. Ryeom HK, Kim SH, Kim JY, et al. Quantitative evaluation of liver function with MRI using Gd-EOB-DTPA. *Korean J Radiol*. 2004;5(4):231–239.
51. Schuhmann-Giamperi G. Liver contrast media for magnetic resonance imaging: interrelations between pharmacokinetics and imaging. *Invest Radiol*. 1993;28(8):753–761.
52. Leonhardt M, Keiser M, Oswald S, et al. Hepatic uptake of the magnetic resonance imaging contrast agent Gd-EOB-DTPA: role of human organic anion transporters. *Drug Metab Dispos*. 2010;38(7):1024–1028.
53. Clement O, Muhler A, Vexler V, Berthezene Y, Brasch RC. Gadolinium-ethoxybenzyl-DTPA, a new liver-specific magnetic resonance contrast agent. Kinetic and enhancement patterns in normal and cholestatic rats. *Invest Radiol*. 1992;27(8):612–619.
54. Evenepoel P, Zeegers M, Segaert S, et al. Nephrogenic fibrosing dermopathy: a novel, disabling disorder in patients with renal failure. *Nephrol Dial Transplant*. 2004;19(2):469–473.
55. Cowper SE. Nephrogenic systemic fibrosis: an overview. *J Am Coll Radiol*. 2008;5(1):23–28.

Supplementary figures

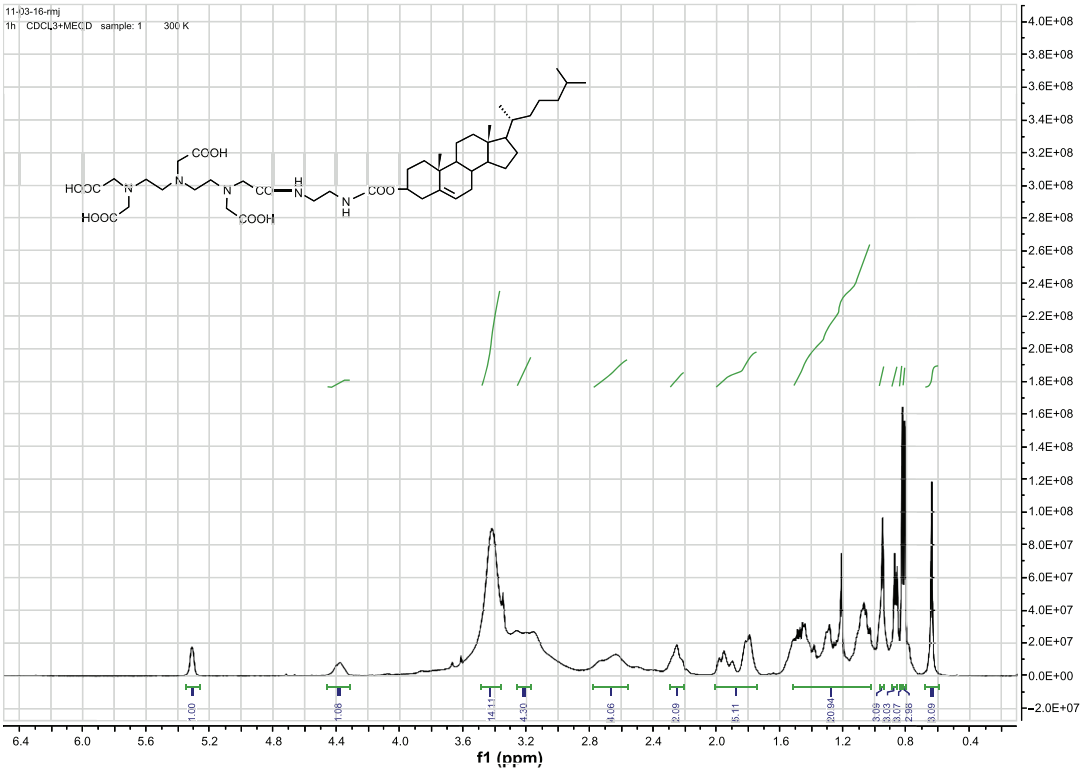

Figure S1 ^{1}H NMR spectrum of DTPA-cholesterol (400 MHz, $CDCl_3$ + drops of CD_3OD).

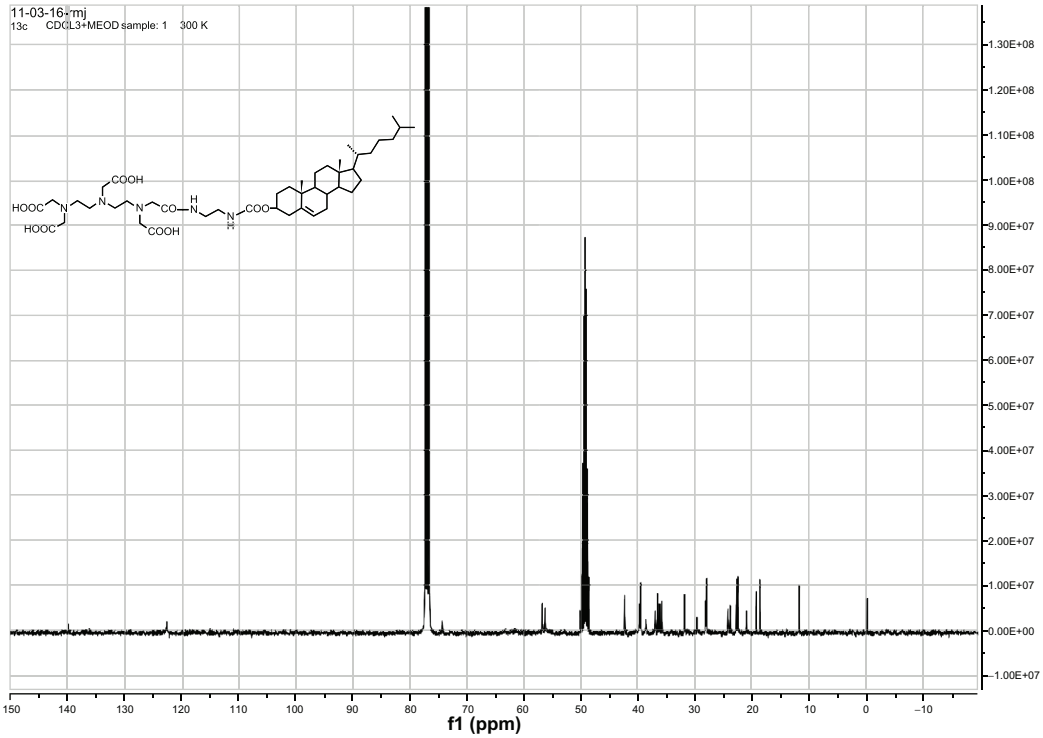

Figure S2 ^{13}C NMR spectrum of DTPA-cholesterol (400 MHz, $CDCl_3$ + drops of CD_3OD).

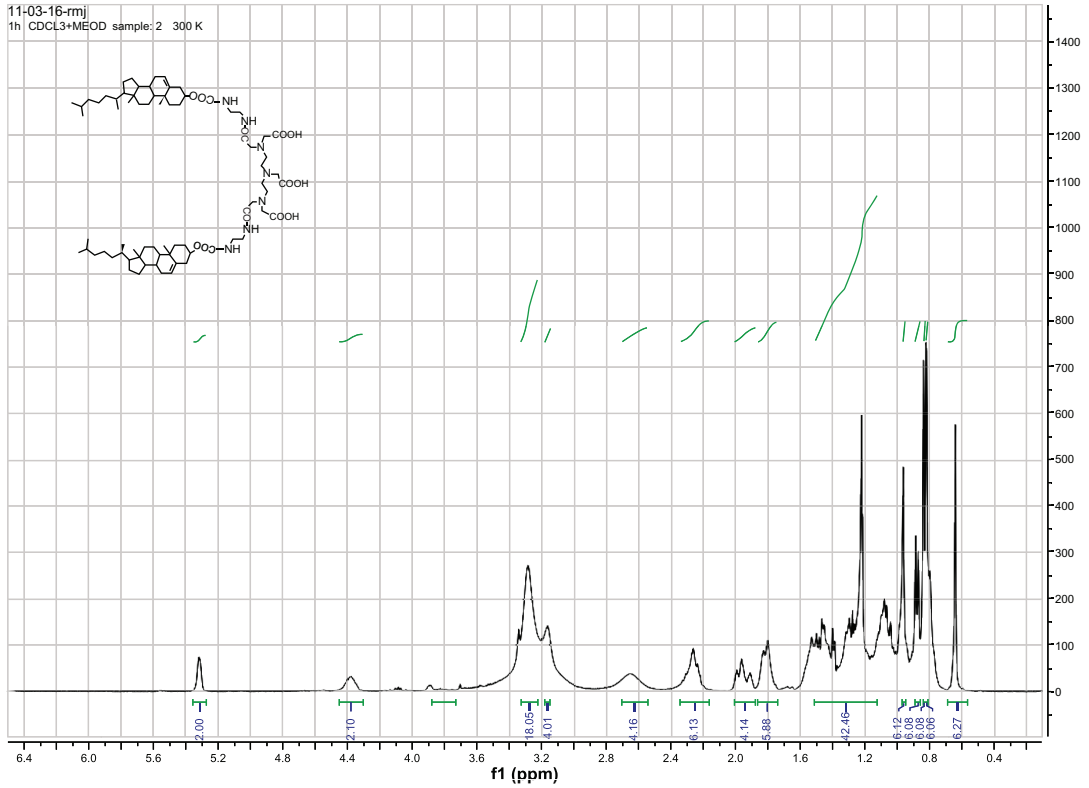

Figure S3 ^{1}H NMR spectrum of DTPA-(cholesterol)$_2$ (400 MHz, $CDCl_3$ + drops of CD_3OD).

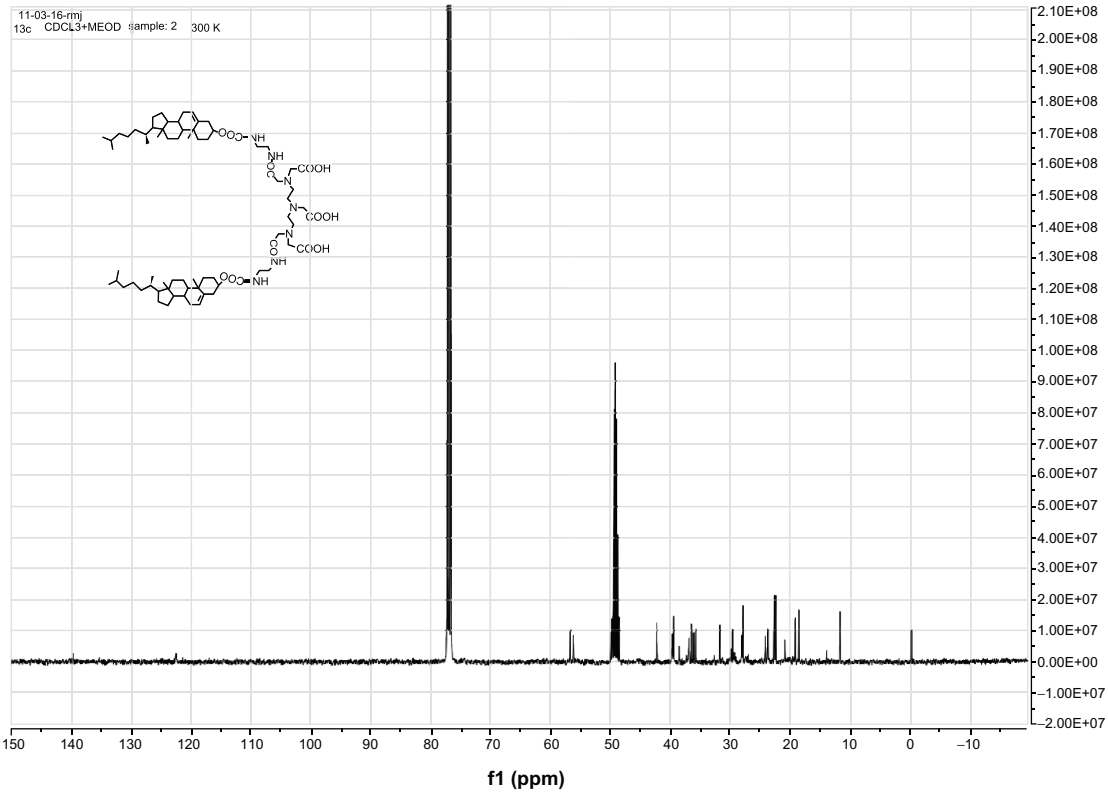

Figure S4 ^{13}C NMR spectrum of DTPA-(cholesterol)$_2$ (400 MHz, $CDCl_3$ + drops of CD_3OD).

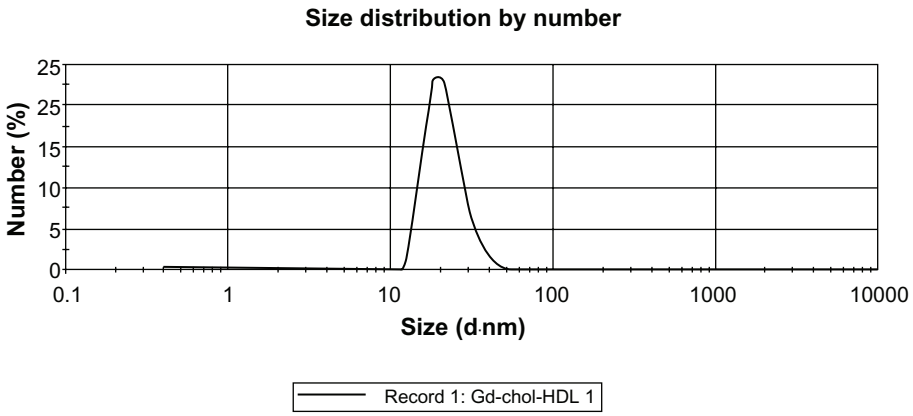

Figure S5 DLS measurement for Gd-chol-HDL (average size 21.74 nm, PDI 0.384).

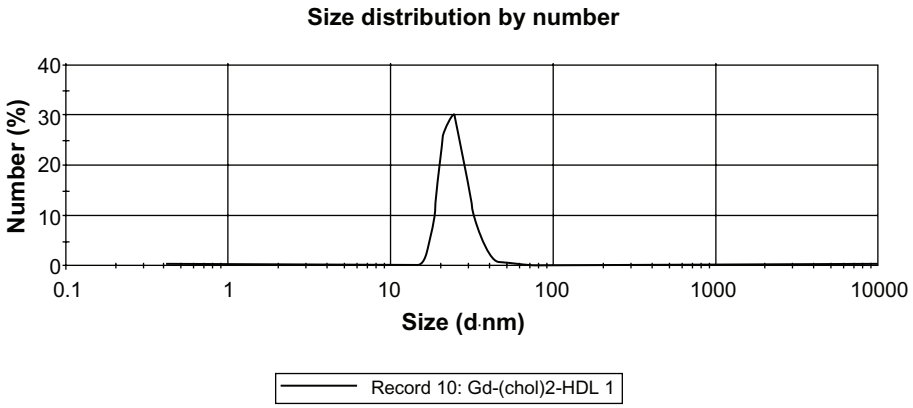

Figure S6 DLS measurement for Gd-$(chol)_2$-HDL (average size 25.54 nm, PDI 0.294).